Taylor & Francis
Taylor & Francis Group

Philosophical Magazine

ISSN: 1478-6435 (Print) 1478-6443 (Online) Journal homepage: https://www.tandfonline.com/loi/tphm20

Characterization of the fracture toughness of micro-sized tungsten single crystal notched specimens

Stefan Wurster, Christian Motz & Reinhard Pippan

To cite this article: Stefan Wurster, Christian Motz & Reinhard Pippan (2012) Characterization of the fracture toughness of micro-sized tungsten single crystal notched specimens, Philosophical Magazine, 92:14, 1803-1825, DOI: 10.1080/14786435.2012.658449

To link to this article: https://doi.org/10.1080/14786435.2012.658449

Published online: 10 Feb 2012.

Philosophical Magazine
Vol. 92, No. 14, 11 May 2012, 1803–1825

Taylor & Francis
Taylor & Francis Group

Characterization of the fracture toughness of micro-sized tungsten single crystal notched specimens

Stefan Wurster*, Christian Motz and Reinhard Pippan

Erich Schmid Institute of Materials Science of the Austrian Academy of Sciences, Jahnstraße 12, 8700 Leoben, Austria

(*Received 28 July 2011; final version received 12 January 2012*)

Fracture experiments using micrometer-sized notched cantilevers were conducted to investigate the possibility of determining fracture mechanical parameters for the semi-brittle material tungsten. The experiments were also used to improve the understanding of semi-brittle fracture processes for which single crystalline tungsten serves as a model material. Due to the large plastic zone in relation to the micrometer sample size, linear elastic fracture mechanics is inapplicable and elastic-plastic fracture mechanics has to be applied. Conditional fracture toughness values J_Q were calculated from corrected force vs. displacement diagrams. Crack growth was accessible by direct observation of *in-situ* experiments as well as with the help of unloading compliances. As a further tool, fracture toughness can be determined via crack tip opening displacement. The micro samples behave more ductile and exhibit higher fracture toughness values compared to macro-sized single crystals and fail by stable crack propagation.

Keywords: tungsten; focused ion beam; fracture mechanics; micro-mechanics; *in-situ* electron microscopy; fracture toughness; crack growth

1. Introduction

Fracture experiments using notched micro-cantilevers have already been performed using a variety of materials. Some of these materials and results [1–6] are summarized in Table 1. It becomes evident that the focused ion beam (FIB) workstation is the most important tool for fabricating small samples. The materials, described in Table 1, are not of outstanding fracture toughness but have a high strength. All results presented for fracture toughness are based on linear elastic fracture mechanics (LEFM); they were determined by using both analytical calculations and finite element simulations. Changing the size of the samples from the millimeter to the micrometer-size regime may alter the fracture behavior especially when testing semi-brittle and ductile materials. For tensile experiments, downscaling is possible, in principle, to any size without changing the experiment and the applied stress state. On the contrary, fracture experiments and the fracture process itself are governed by plastic deformation in front of the crack tip, which spreads out a certain length scale changing the fracture behavior when the sample size is small compared to the plastic

*Corresponding author. Email: stefan.wurster@oeaw.ac.at

ISSN 1478–6435 print/ISSN 1478–6443 online

http://dx.doi.org/10.1080/14786435.2012.658449
http://www.tandfonline.com

Table 1. Summarizing recent results investigating the fracture behavior of various materials using micrometer-sized notched cantilevers.

Material	Ref.	Production and size	Notches	Fracture toughness K_{IC}/K_Q
Lamellar Ti–46Al–5Nb–1W (in at. %, 'Alloy 7')	[1]	FIB, out of thin foils, cantilever measuring about $20 \times 7 \times 36\,\mu m^3$	FIB, depth: less than 5 μm, width: 500 nm	12 samples, $K_Q = 1.4$–$6.9\,MPa\,m^{1/2}$
Ti–48Al, two-phase single crystal lamellas	[2]	FIB-made from foils with a thickness of 20 μm, cantilevers of $10 \times 20 \times 50\,\mu m^3$	FIB, interlamellar and translamellar, width: 0.5 μm, depth: 5 μm	Interlam.: $K_Q = 1.5$–$3.6\,MPa\,m^{1/2}$; Translam.: $K_Q = 5.0$–$8.1\,MPa\,m^{1/2}$
Monolithic Si, prepared to show (111) cleavage plane	[3]	FIB made cantilevers, from bulk material, specimens of pentagonal shape	FIB, line milling with 1 pA, notch width is expected to be in the order of 10 nm	4 samples, $K_{IC} = 1.1 \pm 0.016\,MPa\,m^{1/2}$
CVD-deposited WC coating on a bulk steel substrate	[3]	FIB made cantilevers, from bulk material, specimens of pentagonal shape	FIB, line milling with 1 pA, notch width is expected to be in the order of 10 nm	4 samples, $K_{IC} = 3.2 \pm 0.3\,MPa\,m^{1/2}$
Magnetron sputtered TiN film on single crystalline (100) Si	[4]	FIB, length of cantilevers: 60–77 μm, thickness: 10–10.8 μm, varying thickness of substrate	FIB, depth: 200 nm (50 pA), notch radius: 10 nm	4 samples, $K_{IC} = 2.6 \pm 0.3\,MPa\,m^{1/2}$
Ni–11.5 wt% P amorphous alloy thin films	[5]	FIB, cantilevers: $10 \times 12 \times 50\,\mu m^3$	FIB made notches of 6 μm ($a/W = 0.5$) in length. Fatigue pre-cracks by cyclic compressive loading.	$K_Q = 5.4\,MPa\,m^{1/2}$, large scale yielding
Silicon oxide	[6]	FIB, cantilever, 1.69 (B) × 2.1 (W) × 5.1–5.2 (L) μm^3	FIB, line milling (5 pA), notch root radius ~ 10 nm	2 samples, $K_{IC} = 0.63$–$0.72\,MPa\,m^{1/2}$
Silicon oxynitride	[6]	FIB, cantilevers, 1.65–1.67 (B) × 2.1 (W) × 5.2 (L) μm^3	FIB, line milling (5 pA), notch root radius ~ 10 nm	3 samples, $K_{IC} = 0.91$–$1.00\,MPa\,m^{1/2}$
Silicon nitride	[6]	FIB, cantilever, 1.45–1.61 (B) × 2.1 (W) × 4.9 (L) μm^3	FIB, line milling (5 pA), notch root radius ~ 10 nm	4 samples, $K_{IC} = 1.54$–$1.73\,MPa\,m^{1/2}$

zone size, i.e. there is an inherent length scale in fracture toughness testing. Small scale yielding is a prerequisite for the application of LEFM; hence, the size of the plastic zone, ω, is given by

$$\omega \propto K_{\mathrm{IC}}^2 \Big/ \sigma_y^2. \tag{1}$$

In Equation (1), ω has to be significantly smaller than the length of the crack and sample dimensions in order to apply LEFM. K_{IC} is the critical stress intensity of the material for fracture in mode I and σ_y the material's yield strength, with both material parameters taken at the relevant test temperature. However, at this point, it has to be mentioned that the transition from small scale yielding to full scale yielding is not a specific feature of micro samples, but it can also appear for macroscopic samples, e.g. when fracture toughness is very large or yield strength is low. Formulating the importance of the size of ω in a more accurate way, ω must be smaller than the K-dominated zone in front of the crack. A standard for measuring plane strain fracture toughness values, ASTM E399 [7], sets the lower limit of crack length, a, and sample thickness, B, to $2.5K_{\mathrm{IC}}^2/\sigma_y^2$.

There are micrometer-sized fracture experiments where LEFM can be used to give meaningful results. Matoy et al. [6] investigated the fracture behavior of chemical vapor deposited amorphous silicon oxide, oxynitride and nitride films using FIB-notched cantilevers. The most disadvantageous combination of fracture toughness and measured fracture stress σ_{f} was found for silicon nitride: $K_{\mathrm{IC}} = 1.73\,\mathrm{MPa\,m^{1/2}}$, $\sigma_{\mathrm{f}} = 9.1\,\mathrm{GPa}$. The size of ω was about 10 nm. Here, fracture stress is taken as a lower limit for the yield strength and the un-notched samples did not show any plastic deformation prior to fracture. Thus, crack length and thickness have to be larger than approximately 100 nm to fulfill the requirement given in [7]. These conditions can be kept easily.

In [2], fracture experiments using samples in the micrometer regime made from lamellar Ti–48Al are described. The authors report very low fracture toughness values (1.5–3.6 $\mathrm{MPa\,m^{1/2}}$) for interlamellar crack orientation, i.e. the crack propagation direction is parallel to the lamellae. The lower bound is in accordance to energy calculations for cleavage fracture. For the translamellar crack orientation, where the crack propagation is perpendicular to the lamellae, the fracture toughness was found to be higher (5.0–8.1 $\mathrm{MPa\,m^{1/2}}$) but lower compared to macroscopically large samples ($\sim$20 $\mathrm{MPa\,m^{1/2}}$ [2]). The authors argued that extrinsic toughening mechanisms, e.g. crack bridging, are not activated. Nevertheless, the small specimen size in relation to this comparably high toughness might lead to a reduced value of K_{IC}. So, is the method of using micrometer-sized fracture samples henceforth restricted to materials of limited fracture toughness and high yield stress values?

In the study presented here, the peculiarities of micro-scaled fracture experiments will be discussed and the purpose of this work is to determine the fracture behavior of single crystalline tungsten using micro-sized samples. For the first time, elastic-plastic fracture mechanics will be introduced into this sample size regime. This was done in order to shed light on the fracture behavior of bcc metals in the brittle regime with single crystalline tungsten as a model material. Furthermore, the goal is to better understand fracture experiments on this length scale as these experiments are

quite new and not as elaborate as experiments using large samples dating back through history [8].

Micro-fracture experiments are a very useful tool, as they feature the general possibility of testing single microstructural constituents, like single grains, grain boundaries [9,10], phase boundaries or especially aligned microstructures and multilayer systems [1,2,11]. It is possible to determine parameters describing the fracture behavior of brittle materials [1–6,11]. Within this paper, it will be analyzed if it is also possible for semi-brittle materials.

The manuscript is outlined as follows: Section 2 contains a description of the material used and effects that appear when testing microscopically small samples. Section 3 deals with manufacturing of samples using the ion slicing technique and the FIB. Section 4 is devoted to the evaluation of the experiments based on different fracture mechanics approaches (linear elastic vs. elastic-plastic). Furthermore, it includes a comparison of naturally cracked cantilevers with FIB-notched cantilevers. It tries to answer the question of equivalency. The discussion (Section 5) will focus on a detailed description of the fracture process, which is different to macroscopic samples. In addition, a comparison of results, which were gained from different evaluation processes, is presented.

2. Description of the tungsten crystals and fracture size effects

The material chosen for this work was a tungsten single crystal, a material which is too tough and too soft at room temperature for the successful application of LEFM on micrometer-sized samples (see Equation (1)). Setting the proportionality factor in Equation (1) to $1/\pi$, the plastic zone ω for the tested crack system is about 29 μm; hence, it is larger than the specimens. For comparison, the longest dimension of the cantilevers, used for the experiments described below, is shorter than 10 μm, the initial ligament length, $W - a$, is even smaller, about 2–3 μm (Figure 1). The exact dimensions of all specimens are given in Table 2 and more details on samples and experiments will be given in the Section 3. The yield strength σ_y was chosen to be 650 MPa, according to [12], where tensile experiments on differently sized samples made of electron beam melted tungsten single crystal in [001] direction are described.

The single crystal used for these experiments was aligned in order to test the $\{100\}$-$\langle 011\rangle$ crack system. The notation of the crack system, $\{hkl\}$-$\langle uvw\rangle$, gives the crystallographic plane $\{hkl\}$, wherein the crack is introduced together with the direction of the crack front $\langle uvw\rangle$. Micro-specimens that were made on the basis of the production route and experimental setup described in [13] were used. Macroscopically large samples of the same orientation have the lowest fracture toughness K_{IC} of $6.2 \pm 1.7\,\mathrm{MPa\,m^{1/2}}$ and energy release rate G of $82.5 \pm 55\,\mathrm{N/m}$ at room temperature in comparison to all other crack systems $8.7–20.2\,\mathrm{MPa\,m^{1/2}}$ [14,15].

Another question to be answered: Do micro-scaled experiments allow transfer of fracture mechanical properties from one range of sample sizes (tens of micrometers and below) to the macroscopic range (mm and larger)? What has to be kept in mind is that size effects are present on the micro scale, which was shown, for example, by Uchic et al. [16] for compression samples and Fleck et al. [17] by comparing tensile

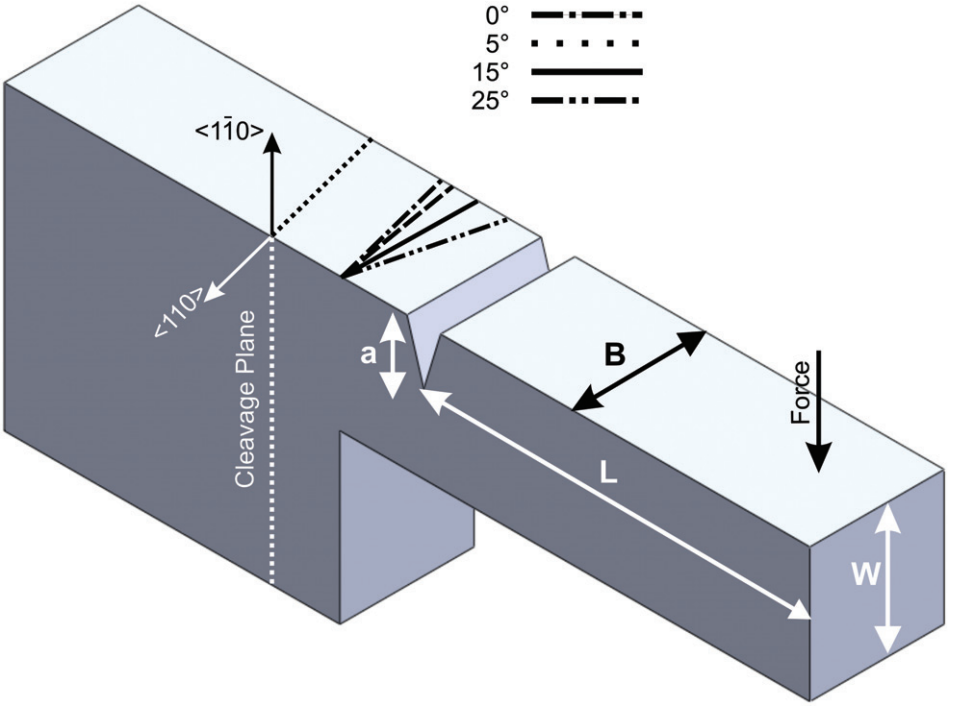

Figure 1. Schematic representation of the general shape of the four FIB-notched cantilevers (S1)–(S4), showing the {100} cleavage plane, the $\langle 1\bar{1}0 \rangle$ direction being anti-parallel to the crack propagation direction and the $\langle 110 \rangle$ direction representing the crack front direction for (S1). Crack length, a, bending length, L, width, B, and specimen thickness, W – as given in Table 2 – are indicated. Furthermore, the point of application of force and the four different notch systems (S1 = 0°, S2 = 5°, S3 = 15° and S4 = 25°) are indicated.

and torsion experiments of thin wires, where they detected an increase in strength with decreasing size. Motz et al. [18] found an even more pronounced effect for micro-sized, FIB-made cantilevers. There was an increase in flow stress with decreasing cantilever thickness, which was explained by a combination of two processes: a decrease in available dislocation sources and dislocation pile-up at the neutral axis of the bending beam. A further explanation might be given by starvation of dislocations due to the high ratio of surface to volume [19,20]. In contrast to these experimentally found facts, Shim et al. [21] reported a pronounced decrease in strength of FIB-made micro-pillars in comparison to as-grown micro-pillars. The decrease is caused by defects, introduced during sample production. Therefore, one ends up with both a decrease in strength that seriously affects the materials fracture behavior via Equation (1), which is due to introduction of defects by specimen production [22] and with an increase in strength due to the small samples size. As a consequence, fracture experiments should be accompanied by tensile tests using samples of the same size and which were subjected to the same production steps (i.e. ion beam milling).

Table 2. Dimensions and crack systems of notched cantilevers. α is the adjusted angle between the normal vectors of notch plane and cleavage plane. L is the maximal bending length, B the sample thickness, W the sample width and a the crack length. Where not stated otherwise, all measurements are taken from SE micrographs. $K_{Q,LEFM}$, $K_{Q,J,Method\ 1}$ (from increasing cantilever compliance), $K_{Q\ J,Method\ 2}$ (from linear fits of J–Δa curves) and $K_{Q,CTOD}$ are the fracture toughness values determined in the corresponding sections.

Specimen no.	Type of crack system	α (°)	L (μm)	B (μm)	W (μm)	a (μm)	$K_{Q,LEFM}$ (MPa m$^{1/2}$)	$K_{Q,J,Method\ 1}$ (MPa m$^{1/2}$)	$K_{Q,J,Method\ 2}$ (MPa m$^{1/2}$)	$K_{Q,CTOD}$ (MPa m$^{1/2}$)
(S1)	{15 1 0} ⟨$\bar{1}$ 15 17⟩	0	9.5	7.2	3.6	1.5	2.9	12.5	12.8	9.2
(S2)	{22 4 3} ⟨$\bar{2}$ 6 7⟩	5	9.4	5.7	4.4	1.4	3.1	13.8	18.4	13.0
(S3)	{29 7 6} ⟨$\bar{9}$ 19 22⟩	15	9	5.2	4.4	1.8[a]	3.7[b]	14.4	20.9	13.1
(S4)	{26 10 9} ⟨$\bar{13}$ 16 19⟩	25	9.6	3.8	4.4	1.5	3.5	15.5	22.3	14.4

Notes: [a]Not according to SE micrograph for determination of crack length; crack length was determined from first unloading stiffness (see Appendix). [b]F_{max} instead of F_Q was used for determination of a conditional stress intensity value.

For both types, macro-samples and micro-samples, a crack has to be introduced or already be present. This can be done with cyclic loading, as is described by standards [15,23–26], and is also possible on the micro scale [5]. However, the majority of the published scientific work relies on the introduction of a small notch with the FIB, e.g. using the line milling mode with low currents in the pA regime. References [3,4,6] report crack tip radii of about 10 nm, when using ion currents of 1 pA to 50 pA. For the investigations described here, currents of 50 pA to 100 pA were used. The question, whether a FIB-made notch is equivalent to a natural crack still lacks a final answer. This publication tries to answer it by comparing the fracture behavior of FIB-notched cantilevers with the fracture behavior of single crystalline tungsten specimens containing a natural crack.

3. Sample preparation and experiments

The production of micrometer-sized specimens is outlined explicitly in [13], so only a short summary will be given here. An ion slicer (JEOL EM-09100IS) is used to remove large amounts of material, altering its actual purpose of transmission electron microscopy sample production. Low energy argon ions with a maximum energy of 6 keV are used. The result of the ion slicing process is a thin lamella a few micrometers in thickness and up to about one millimeter in length. This lamella is used as a preform for further processing. Subsequently, any desirable sample shape (tensile, compression, bending) using a FIB workstation (LEO XB 1540) is possible.

Several notched cantilevers were made; their dimensions and crack system are outlined in Table 2. Gallium ion currents for cutting the sample contours were 500 pA to 2 nA, ion currents of 50 pA to 100 pA were used for cutting the notches using the line-milling mode. Acceleration voltage was 30 kV for all milling steps. No fatigue pre-cracking of cantilevers, such as that described in [5], was conducted. The notches of cantilevers (S1)–(S4) were aligned with certain deviations with respect to the cleavage plane (Figure 1). The misorientation of cleavage plane and FIB-notch plane (quantity α in Table 2) was increased from $\sim 0^\circ$ (S1), 5° (S2) and 15° (S3) to 25° (S4). Furthermore, the crack systems of all cantilevers are outlined in Table 2. The principal idea of this procedure was to obtain increasing fracture toughness values for increasing misorientations, thus to check consistency of the methods of evaluation. All notches were cut with the line milling mode into the top surface by use of defined milling times. By changing the milling time, it was possible to adapt the notch depth. Using a milling time per length of milling line of 40 s/μm (20 μm/s) and an ion current of 50 pA (100 pA) in line milling mode resulted in a notch depth of approximately 1.5 μm.

Electron backscatter diffraction (EBSD) measurements, which were made on the surface of the lamella, were necessary to obtain knowledge on the crystal cleavage system. The software OIM – Orientation Imaging Microscopy v5.31 was used. Due to the sequence of manufacturing steps (cutting, ion slicing and mounting of crystal on sample holder and within the SEM), the cleavage system does not coincide with the perpendicularity of the lamella. It is necessary to tilt the notches, as can be seen in Figure 1 for (S1)–(S4). Tilting of 15° in one directions results in coinciding cleavage and crack systems (S1); tilting of 10° in the opposite directions results in the largest

difference between both systems (25°, S4). With increasing deviation of the notch plane from the ideal cleavage plane there is a change of the crack front direction from ⟨110⟩ to ⟨111⟩. The crack propagation direction was the same for all specimens and it was always very close to $\langle\bar{1}10\rangle$. According to EBSD analysis it was of ⟨17 15 1⟩-type. What has to be mentioned when referring to EBSD measurements is the fact that relative misorientations within a single specimen can be determined at rather high accuracy, below 1°. However, absolute values incorporate higher inaccuracies, especially as the crystallography was measured by EBSD. The samples were transferred to the FIB for cutting and mounted inside a scanning electron microscope (SEM) for *in-situ* testing. Consequently, a perfect alignment of loading direction towards the notch plane, which should then again be ideally positioned at a certain defined deviation from the cleavage plane, is unlikely. Inaccuracies within a few degrees are expected. Henceforth, the four crack systems of the cantilevers (S1)–(S4) will be described by the FIB-adjusted deviations of the notch plane from the cleavage planes.

Cantilevers were loaded *in-situ* in a SEM (LEO 982) using a micro indenter (ASMEC, UNAT) with a cube corner tip. Loading and unloading speed was set to 1 μm/min for all specimens, including the ones incorporating natural cracks ((NC1) and (NC2)). Stable crack growth was observed for all cantilevers and, as a consequence, J–Δa curves and CTOD–Δa curves can be drawn. This will be done in Section 4.2, which describes the elastic-plastic fracture mechanics approach. Force and indenter displacement were recorded and the results for specimens (S1)–(S4) are shown in Figure 2a. Several unloading steps during the experiment allowed the measurement of crack extension due to the decreasing cantilever compliance. The automatic recording of several thousand scanning electron (SE) micrographs for one single experiment resulted in detailed knowledge of the fracture progress.

To investigate whether a difference exists between a FIB made notch and a natural crack, experiments were also carried out using cantilevers incorporating natural cracks. To perform this work, two specimens were produced out of bulk tungsten single crystal. Due to the cutting of the single crystal, a large number of surface cracks evolved, showing the typical fish scale pattern (Figure 3). The cantilever top surface is of {111}-type and according to results on experiments introducing cracks in tungsten single crystals by electrical discharge machining the crack planes are most likely of {100}-type [27,28]. Without using the ion slicing process, as this would most likely eliminate the near-surface cracks, a thin lamella was produced with the FIB [18]. It is important to emphasize that the crack front did not experience any FIB damage, except at the points where it penetrates the lateral surfaces. Gallium ion damage of the lateral surfaces should be less an issue.

4. Results

4.1. *Linear elastic fracture mechanics approach*

The conditional critical stress intensity, K_Q, for notched cantilevers is derived according to [7,29]:

$$K_Q = \frac{F_Q L}{B W^{3/2}} f(a/W), \tag{2}$$

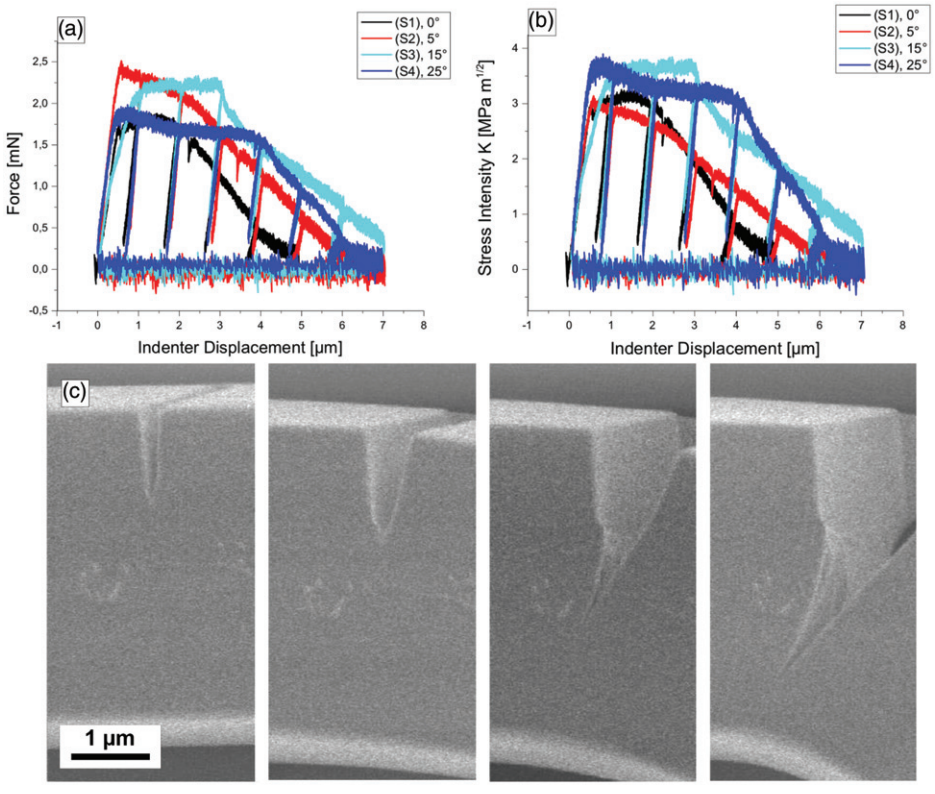

Figure 2. (a) Measured force vs. indenter displacement for (S1)–(S4); (b) corresponding stress intensity factors at the crack tip based on LEFM and Equations (2) and (3) without considering crack propagation. (c) A sequence of SE micrographs of cantilever (S2), which correspond to the starting point without any load applied and further on the moment before the 2nd, 4th and 6th unloading.

where

$$f(a/W) = 4\frac{\left\{\begin{array}{l} 3(a/W)^{0,5}(1,23-(a/W)(1-(a/W)) \\ \quad (-6,09+13,96(a/W)-14,05(a/W)^2)) \end{array}\right\}}{2(1+2(a/W))(1-(a/W))^{1,5}}, \tag{3}$$

F_Q is the force determined according to ASTM E-399 [7], L the bending length, a the crack length, B the thickness of the specimen and W the width of the specimen. The shape factor $f(a/W)$ for the sample geometry used was calculated by using two-dimensional ABAQUS finite element simulations via the procedure outlined in [29]. No inclination of the FIB-notch plane was taken into account. However, as the angles of inclination are small, the same shape factor $f(a/W)$ was used for all cantilevers. The specimen dimensions were measured using SE microscopy and, with Equations (2) and (3), stress intensity factors, K, were determined (Figure 2b). F_Q and K_Q are presented together with specimen dimensions in Table 2. For specimen (S3), a change of slope during initial loading took place and might be attributable to the breaking of a thin

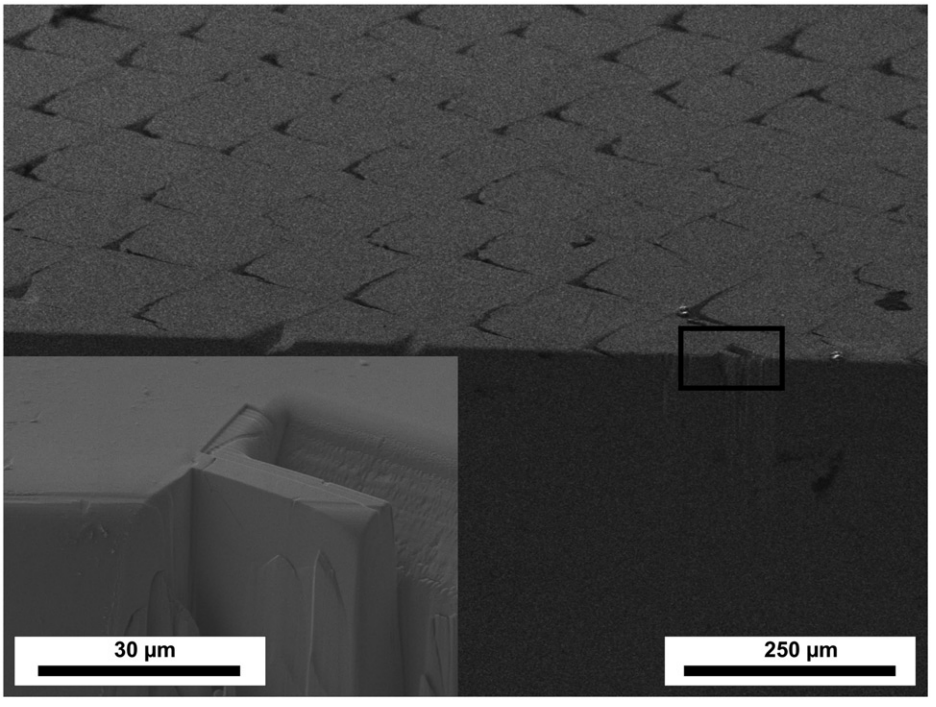

Figure 3. SE micrograph, showing an inclined view on the surface of the tungsten single crystal containing the surface cracks. They are arranged in the typical fish scale – pattern. The inlay shows a cantilever in its semi-finished state, depicting the arrangement of both cantilevers, (NC1) and (NC2) in relation to the cracks.

wall, being a remnant from FIB-notching. Consequently, for (S3) the initial slope of loading cannot be used to determine K_Q; instead $K_{\max}$ was taken.

All six samples ((S1)–(S4), (NC1) and (NC2)) do not ful fill the requirements that are given by standards determining the measurement of plane strain fracture toughness; thus, the results will be presented as conditional fracture toughness values, indicated with the subscript "Q". The depiction of K (Figure 2b) does not take into account any crack propagation nor any large-scale yielding and leads to the fact that critical stress intensities do not represent valid values but only lower limits. The actual minimum limit for sample size according to [7] would be about 230 µm; this requirement is missed by about two orders of magnitude. However, using LEFM is sufficient for the determination of mechanical properties for small components, as it results in a complete description of the reaction of a specimen to a load. In contrast, it is not sufficient to derive valid fracture properties from small samples. For large-scale yielding, other methods have been successfully applied for macroscopic samples and fracture toughness can be determined using J-integrals, crack tip opening displacement (CTOD) or crack tip opening angle (CTOA). Stable crack growth is observable via the compliance method or potential drop method. These approaches will be presented in the next subsection.

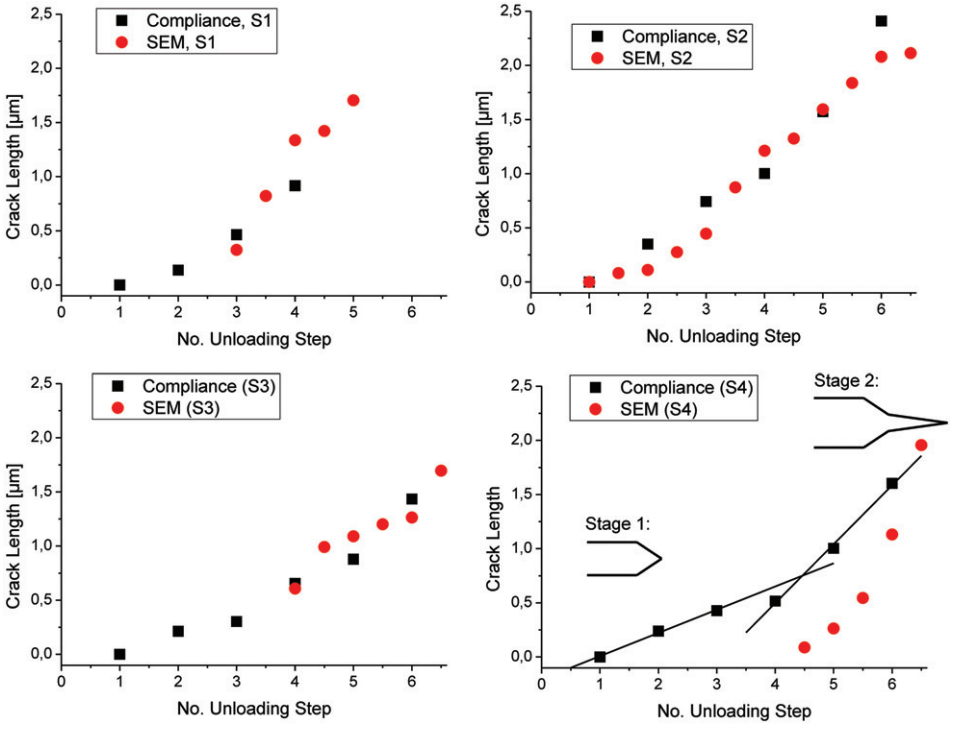

Figure 4. Comparison of crack lengths for cantilevers (S1)–(S4), measured in SE micrographs at points in time corresponding to the beginning of the unloading procedure and in micrographs taken in between two unloading procedures (red points). Black squares represent crack lengths determined by use of the compliance method, Equation (4). For cantilever (S4), the two different regimes of crack propagation, as discussed in Section 5, are indicated. The unloading steps are performed at equidistant displacment.

4.2. *Elastic-plastic fracture mechanics approach*

4.2.1. *J-integral*

Ion slicing aids in reducing the time to manufacture the cantilevers, as they do not have to be cut out from bulk material. Thus, in principle, a multiple specimen technique for determination of *J*-values could be used. However, due to the complexity of the experiments, it is recommended to use a single specimen technique for determination of the *J*-integral. This requires detailed knowledge on the crack extension during the experiment, which can be achieved in two ways. First by the unloading compliances of the cantilevers and secondly by *in-situ* observation of the fracture process and crack growth. Both methods will be described in the appendix and the results are depicted in Figure 4. Force vs. displacement diagrams serve as a basis for the determination of *J*-values. However, the recorded data of force and displacement has to be corrected regarding compliance of the lamella the cantilevers are located on, and the indentation of cantilevers. Details on data correction can also be found in the appendix.

The actual ASTM standard for the determination of the J-integral [24] relies on the very detailed knowledge of the crack extension. Of course, it would be feasible to perform a large number of unloading steps but one would then end up with a low cycle fatigue experiment rather than fracture experiments. Henceforth, J-values will be calculated using an old standard [26]. $J_{(i)}$ at the ith point of unloading is given as the sum of elastic and plastic components:

$$J_{(i)} = \frac{(K_{(i)})^2(1-\nu^2)}{E} + \frac{\eta A_{Pl(i)}}{B(W-a_0)}, \tag{4}$$

where $K_{(i)}$ is determined by Equations (2) and (3), η is a constant factor equal to 2 and ν is the Poisson's ratio, which was 0.28. $A_{Pl(i)}$ represents the area beneath the load vs. displacement curve, excluding a triangle that is defined by the unloading line. For each unloading step the according crack length and J-integral is determined and presented in Figure 5a showing J versus crack extension, the J–Δa curve.

All J–Δa curves in Figure 5a show the typical shape that is also observed for macroscopic tests of ductile materials. The J–Δa curve should then be fit using a power law of the form [24]:

$$J(a) = C_1\left(\frac{\Delta a}{k}\right)^{C_2}. \tag{5}$$

In Equation (5), k is a constant and C_1 and C_2 are determined by the fitting procedure. An intersection of this curve with a parallel line to the blunting line has to be made, where the blunting line is a straight line showing the initial slope of the J–Δa curve. This parallel line to the blunting line should be drawn at an offset value for crack extension of 0.2 mm [24], but is not possible for experiments on this length scale. Other possibilities to evaluate the J–Δa curves are needed and two of them will be presented in the following paragraphs.

The first way to evaluate the J–Δa curve is to determine the uppermost value of $J_{(i)}$ where crack extension already took place. For all specimens (S1)–(S4) this is before the second unloading step, which becomes obvious due to an increased compliance at the second unloading compared to the first unloading. Of course, it is also possible that crack propagation took place in advance of the first unloading step.

The second method to determine critical J-integrals is to fit the set of data shown in Figure 5a with two linear functions. The first function describes the blunting line, i.e. the summarized initial parts of all four J–Δa curves, and the second function the individual slopes of the final part of each J–Δa curve. The slope of the initial linear fit (1417 MPa) is in very good agreement with the slope of the construction line that needs to be drawn according to standard ASTM 1820 [24]. This would then give a slope of 1300 MPa ($=2\sigma_y$), which is a hint for the applicability of the chosen yield strength value. As an example for the second linear function, the linear fit of the final part of cantilever (S4) is depicted in Figure 5a. The intersection of both straight lines gives the J-value at the transition from one stage of fracture to the other and shall serve here as a basis for determination of fracture toughness. This process will be discussed in detail in the next section.

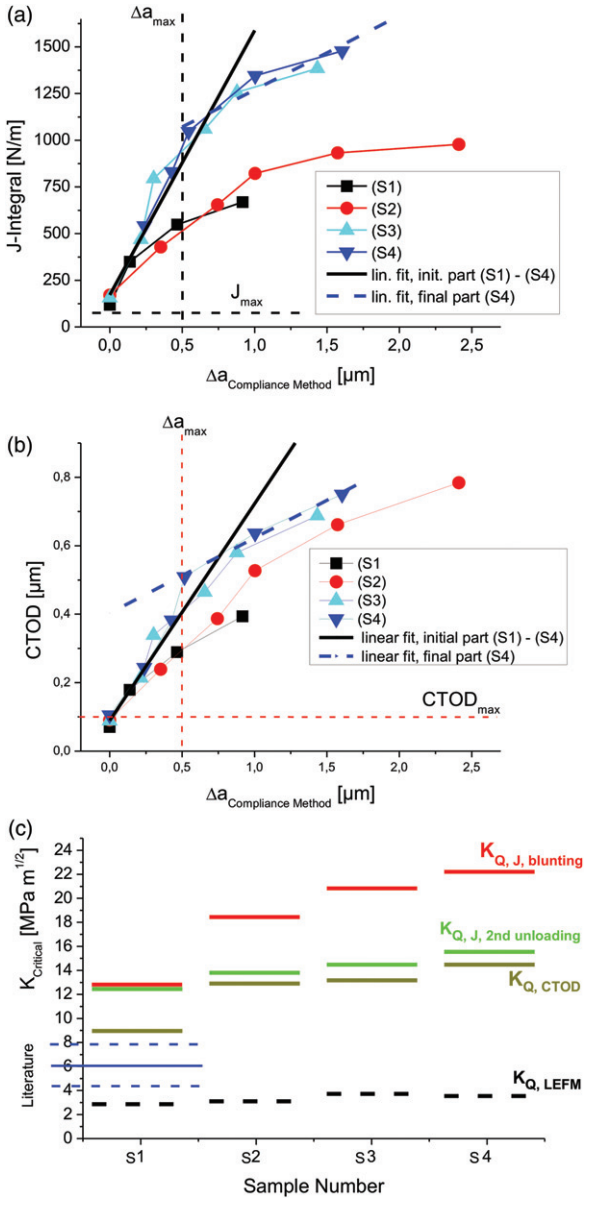

Figure 5. (a) *J*-integral vs. crack growth, Δa, (J–Δa curves) for all notched cantilevers. (b) CTOD versus crack growth Δa (CTOD–Δa curves) for all FIB-notched cantilevers (S1)–(S4). Δa was determined from unloading stiffnesses. The maximum allowed values based on the smallest specimens dimensions in Table 2 for crack extension J and CTOD are outlined in black and red, dashed lines. The blunting lines, being a linear fit of the combination of all initial parts of the curves, are shown as black lines. The blue, dashed lines in (a) and (b) are linear fits of the final part of results of specimen (S4). (c) Compilation of results of conditional fracture toughness values. The elastic–plastic results overestimate the toughness according to LEFM-results from Riedle et al. [14,15], which are also presented in blue for the crack system matching to cantilever (S1).

Fracture toughness $K_{Q,J}$ can be calculated using:

$$K_{Q,J} = \sqrt{\frac{JE}{1-\nu^2}}. \tag{6}$$

For the first method, using the first decrease in compliance, the fracture toughness values were calculated to be 12.5 MPa $m^{1/2}$, 13.8 MPa $m^{1/2}$, 14.4 MPa $m^{1/2}$ and 15.5 MPa $m^{1/2}$ for increasing misorientation from the cleavage plane, respectively. The second method leads to fracture toughness values of 12.8 MPa $m^{1/2}$, 18.4 MPa $m^{1/2}$, 20.9 MPa $m^{1/2}$ and 22.3 MPa $m^{1/2}$ for increasing deflection from the cleavage plane. The results from both models presented in this section are summarized together with the results from LEFM and crack tip opening displacement (Section 4.2.2.) in Figure 5c and in Table 2.

The used standard E813 [26] restricts the initial ligament size $(W-a_0)$ and the thickness B to be greater than

$$(W-a_0), B > \frac{25J_{IC}}{\sigma_Y}, \tag{7}$$

with J_{IC} being the critical value describing the onset of stable crack extension. The smallest dimension of cantilever (S1), $W-a_0$, is 2.1 μm leading to a maximal acceptable J_{IC} value of 55 N/m, again using 650 MPa for σ_y [8]. The J-value corresponding to the first unloading is 119 N/m. The smallest relevant dimension of cantilever (S4) is 2.9 μm leading to a maximal J_{IC} value of 75 N/m. The J-value corresponding to the first unloading is 229 N/m. The requirements are not met by two orders of magnitudes as for LEFM but by a factor of two to three. The maximum crack extension for determination of valid J-values is, as for crack tip opening displacement $(W-a_0)/4$. Taking the smallest value for $W-a_0$ appearing in Table 2, this would result in a conservative limit of about 500 nm. The limit is indicated in Figure 5a with a parallel line to the y-axis.

4.2.2. *Crack tip opening displacement*

Beside the possibility to measure critical J-values, it is also possible to use the crack tip opening displacement as a parameter describing the fracture toughness of the material. For this work, the determination of CTOD is based on a hinge model, which is adopted for notched cantilevers (see Figure 6). The model was proposed in a British standard [25], where the blunting of a 3PB bending sample is assumed to occur by a rotation and the center of rotation is at a depth of $0.45(W-a)$ below the notch front.

Determination of the bending angle Θ results from a combination of corrected indenter displacements at the beginning of the unloading segments in combination with the mean bending length. CTOD versus crack growth curves, i.e. CTOD–Δa curves, were evaluated and are shown in Figure 5b. Crack extensions were determined via the unloading stiffness, as described in the appendix.

The maximum allowed value of CTOD is $(W-a_0)/20$ and $(W-a_0)/4$ is the maximum value for crack extension according to [26]. Conservative values for these limits are $\mathrm{CTOD}_{\mathrm{max,conservative}} = 100$ nm and $\Delta a_{\mathrm{max,conservative}} = 500$ nm, respectively. They are included in Figure 5b as parallel lines to the CTOD and Δa axes. The final parts of the curves in Figure 5b are not with in the limit for Δa and the limitation in

CTOD is even more restrictive. According to ASTM E1820 [24], the initial ligament length must be 35 times larger in order that $CTOD_C$ is a size-independent value, which is not the case here. Nevertheless, the curves show an increase in CTOD with crack extension.

As was proposed in the previous section for the J–Δa curve, the CTOD–Δa curve should be fit according to a power law fit. Again, determination of a critical crack tip opening $CTOD_C$ is not possible due to sample size; thus, $CTOD_Q$ values are given. Proposing another way of evaluation, one single line is drawn for all cantilevers, derived by fitting the initial two to three CTOD-values of all specimens. This line represents the blunting line. The slope of this line (0.63) is smaller by about a factor of two compared to the slope of the construcion line (1.4) proposed by ASTM 1820 [24], thus, indicating a different blunting behavior compared to ductile materials. The fitted line is intersected with individual fitted lines of the final parts of each CTOD vs. Δa curve. The point of intersection gives a result for the conditional crack tip opening displacement $CTOD_Q$ and it is then possible to determine $K_{Q,CTOD}$ using Equations (8) and (9). No hardening is observed; therefore, assuming an elastic–perfectly plasitc material behavior, the relationship between J and CTOD is given by [30]

$$\mathrm{CTOD} = d_n {}^{J}\!/_{\sigma_y}. \tag{8}$$

By use of Equation (7)

$$K_{Q,\mathrm{CTOD}} = \sqrt{\frac{1}{d_n}\sigma_y E' \,\mathrm{CTOD}_Q}, \tag{9}$$

where E' is the reduced modulus that is contained in J and d_n is the Shih factor, which is 0.78 for plane strain conditions [30], the fracture toughness can be calculated. Increasing crack tip opening displacement, $CTOD_Q$, with increasing deviation of notch plane from cleavage plane was observed. $CTOD_Q$ were determined to be 230 nm, 470 nm, 480 nm and 570 nm for the cantilevers (S1)–(S4), respectively. The resulting fracture toughnesses of 9.2 MPa $m^{1/2}$, 13.0 MPa $m^{1/2}$, 13.1 MPa $m^{1/2}$ and 14.4 MPa $m^{1/2}$ are depicted in Figure 5c. What has to be kept in mind is the question of transferability of yield strength from the macro-to micro-regime. Assuming an increase in yield strength due to a size effect, would on the one hand decrease the required sample sizes (Equations (1) and (7)), but on the other hand increase the fracture toughness values derived from CTOD.

4.3. *Naturally cracked cantilevers*

Figure 7a depicts force vs. corrected indenter displacement diagrams for the cantilever (NC2). There is a decrease of the cantilever stiffness, thus, crack propagation takes place. Again, no catastrophic failure was observed, but stable crack growth was observed for (NC2). In contrast, no significant decrease in cantilever stiffness was visible for (NC1). The crack line at the cantilever's top surface was perpendicular to the side surfaces. However, the natural crack did not propagate perpendicular to the surface but at an inclined angle (Figure 8).

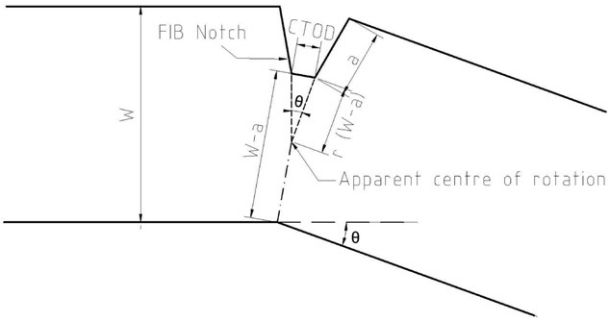

Figure 6. Hinge model adapted to micrometer–sized notched cantilevers.

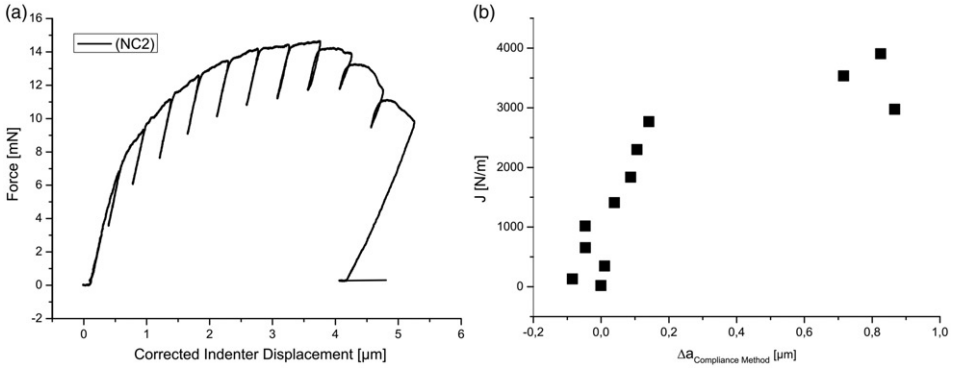

Figure 7. (a) Measured force vs. indenter displacement curve for cantilever (NC2) showing noticeable crack growth. Unloading step hysteresis in the lattter stage of the experiment might be related to crack closure events due to the rough fracture surface. (b) J vs. Δa for (NC2) – the cantilever experiencing crack propagation – shows the same qualitative behavior as it was observed in Figure 5a.

To evaluate mode I fracture toughness values, the cantilever would have to be cut and tested at a certain angle with respect to the single crystal's top surface. This would make production and testing more complicated and was not performed.

The first important statement is that there is no qualitative difference in the fracture behavior of the FIB produced notches and natural cracks according to load vs. displacement curves. It can be expected that FIB-notched samples deliver equivalent fracture toughness results as naturally cracked samples of the same testing geometry. The fracture toughness value determined by use of LEFM is 4.3 MPa $m^{1/2}$ for (NC2). However, the condition of $F_{max}/F_Q \leq 1.1$ stipulated in [7] is not fulfilled. What has to be taken into account is the inclined starting crack plane and pure mode I loading conditions are not ful filled. Furthermore, the starting crack length is not constant over the specimens' thicknesses but it decreases for (NC1) and increases for (NC2) when starting from the front surfaces visible in Figure 8.

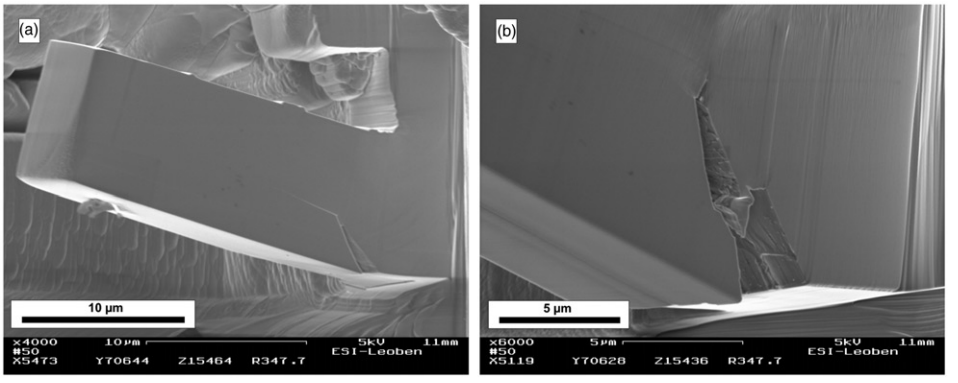

Figure 8. (a) Post-mortem SE micrograph that shows the indent and limited crack propagation of specimen (NC1). (b) Post-mortem SE micrograph of specimen (NC2), which shows crack propagation (~1 μm) and crack deflection from the initial crack plane.

It is possible to determine the effective stress intensities acting at the crack tip of the inclined notches when taking into account additional mode II loadings due to the crack deflection. Since LEFM is not applicable, such mixed mode analyses have not been performed. Elastic-plastic evaluation of cantilever (NC2) according to Section 4.2.2 includes determination of crack growth via decrease in unloading stiffness and the results are presented in Figure 7b. It shows the same trend as depicted in Figure 5a for smaller FIB-notched cantilevers. However, the values of J are larger by about a factor of 2 to 4. A reason for this might be the disadvantageous geometry, crack deflection and the change in loading conditions to a mixture of modes I and II. Despite the differences between natural cracks and FIB-made notches, these experiments lead to the conclusion that the essential fracture behavior of such micro samples is not significantly affected by the FIB-notching.

5. Discussion

5.1. *Fracture process*

The fracture process can be explained by taking into account an idea proposed by Hirsch et al. [31]. They presented a model for stable crack growth by micro-cleavage in semi brittle materials. The model is based on the emission of dislocations directly at the crack tip on crystallographic planes that intersect the crack tip. In principle, it should also be possible that dislocations are emitted on planes in advance of the crack tip if dislocation sources are present. On these planes, regardless of being in front of the crack tip or intersecting the crack tip, shielding as well as anti-shielding dislocations are emitted. Anti-shielding dislocations force the crack to grow due to large tensile stresses, i.e. crack opening stresses. Shielding dislocations move away from the crack tip and in case of cantilever bending, they pile up at the neutral bending axis. However, very little hardening is observed (Figure 2a), hence, the process of dislocation multiplication is considered to be controlled by dislocation

generation at or near the crack tip. Interaction of generated dislocations does not seem to be the controlling process.

It is obvious when comparing Figures 2a, 5a and 5b that two different stages of crack propagation are present during the experiments. The change in type of fracture process manifests as a marked load drop at different stages of the experiment and is more pronounced for cantilevers (S3) and (S4) and less pronounced for cantilevers (S1) and (S2). These load drops appear after the second unloading for (S1) and (S2), after the third for (S3) and after the fourth for (S4). Furthermore, two different slopes of crack length versus the number of equidistant unloading steps depict this effect in Figure 4.

The change of slope in Figure 5b, showing CTOD–Δa curves, is very informative concerning the shape of the crack front and the blunting behavior. The local crack tip opening angle ($CTOA_{local}$) helps to separate the CTOD–Δa curves into different sections and to discuss them separately. $CTOA_{local}$ is defined as

$$CTOA_{local} = 2\tan^{-1}\left(\frac{\Delta CTOD/2}{\Delta(\Delta a)}\right). \tag{10}$$

This approach, using $CTOA_{local}$ gives an idea about the local, thus, crack extension-dependent, shape of the crack tip. In contrast, the angle Θ that was introduced in Section 4.2.2 represents an averaging CTOA, which leads to a smearing out of shape changes of the crack tip. The linear fit of the initial part, shown in Figure 5b, shows that $CTOA_{local}$ for (S1) and (S2) is slightly below the mean value. $CTOA_{local}$ for (S3) and (S4) is somewhat above the mean value of 33°. In other words, the first stage of the fracture process showing high $CTOA_{local}$ can be explained by crack tip blunting and dislocation emission together with a small amount of nano-cracking. Blunting is more pronounced for specimens having a larger misalignment towards the cleavage plane. $CTOA_{local}$ is smaller in the second stage and it seems to be independent of notch deviation. The resulting shape of the crack is depicted as inlays in Figure 4. The transition from blunting to stable crack propagation goes with the above-mentioned load drops. They appear in later stages of the experiments for a higher misorientation between notch- and cleavage-plane. Furthermore, the later the transition from stage 1 to stage 2, the more pronounced the load drop.

The most obvious difference between microscopic and macroscopic fracture experiments is the change in fracture behavior from unstable in large samples to stable in smaller ones. Due to the small sample size, there is only very limited volume containing stored elastic energy. Upon crack propagation, less elastically stored energy is released, which stabilizes the crack propagation during the second stage. Stable crack propagation, though, is not completely new for experiments on single crystalline tungsten. Hull et al. [27] performed fracture experiments using tensile specimens made of small sheets of arc-melted single crystalline tungsten. The tensile axis was in the [010] direction and micro-cracks were introduced on a (010) plane by the spark-machining technique. The samples had a rectangular cross section, 1.2 mm in width and 0.5 mm in thickness. By use of samples having the same crack length of 0.08 mm, they found stable crack propagation for testing temperatures of 22°C and above. After a certain amount of slow crack growth, whose extent increased with increasing testing temperature, the samples finally failed by catastrophic cleavage on

planes of {100}-type. The first stage of blunting and nano-cracking is supposed also to be present in macroscopic samples. The second stage of stable fracture emerges in rare cases for large samples (e.g. [27]), when catastrophic fracture does not take place.

Further experiments will focus on changing the energy release rate of crack propagation. Even smaller samples shall be tested using a pico-indenter of high resolution in force and displacement. Larger samples in the regime of tens of micrometers will be produced using an improved method of argon ion polishing. By alteration of sample size, there is a change in the amount of elastically stored energy. With an increase in volume, one can expect a change from stable to unstable crack propagation in order to find the transition in fracture behavior from micro- to macroscopic samples.

5.2. *Evaluation of fracture toughness*

When summarizing the results from different fracture mechanics approaches presented in Section 4, it can be stated that, as expected, LEFM does not deliver correct fracture toughness values, rather only a lower bound for critical stress intensities. This is attributable to the small sample size, which fails to fulfill the requirements given by testing standards on fracture toughness measurements. However, the values of K_Q deliver good approximations for the first deviation of the curves from ideal elastic behavior indicating a massive emission of dislocations and pronounced plastic deformation. Using a combination of finite-element and atomistic analysis, Kohlhoff et al. [32] found critical stress intensities for the initiation of plastic instabilities (twinning, dislocation emission) in the range of $1.73\,\mathrm{MPa\,m^{1/2}}$ to $2.02\,\mathrm{MPa\,m^{1/2}}$ for various non-cleavage planes. For the cleavage plane investigated in [32], the lower bound for the stress intensity leading to dislocation emission is given by $1.73\,\mathrm{MPa\,m^{1/2}}$ [32]. At the same time, this is the critical stress intensity for crack propagation. The experimentally determined K_Q values (Table 1) are higher by about $1\,\mathrm{MPa\,m^{1/2}}$ (i.e. $\sim 3\,\mathrm{MPa\,m^{1/2}}$). This can be attributed to the comparatively blunt crack tip and the non-detection of the first onset of dislocation emission but only of massive plastic deformation.

CTOD was evaluated by use of the hinge model presented in Figure 6. Critical CTOD-values were determined by linear interpolation of data in Figure 5b and an increasing toughness with increasing deviation of notch plane from cleavage plane and the ideal crack front direction was found. The $K_{Q,\mathrm{CTOD}}$ value for (S1), $9.2\,\mathrm{MPa\,m^{1/2}}$, is beyond the upper bound of $6.2 \pm 1.7\,\mathrm{MPa\,m^{1/2}}$ [14], which was found for large specimens. In this publication, samples of equivalent crystallography to (S1) were tested. Toughness values were determined by use of CTOD values, which depend on the yield strength of the material. As already mentioned, it is important to support the small-scale fracture experiments with tensile tests using specimens produced in the same way. The matching slopes in the J–Δa curves are an indicator that the yield strength of 650 MPa [8] is applicable. On the other hand, a different shape of the blunted crack tip should have been observed with CTOD being about 1.4 times the crack propagation [24], which was not found in the case of small-scale tungsten samples. Fracture toughness values from the J approaches are higher

than $K_{Q,CTOD}$. Comparing both J approaches, the values resulting from the one involving linear fits of the J–Δa curves are higher compared to K_Q values, which were determined by the use of second unloading steps. Conditional fracture toughness values for single crystal tungsten in its most brittle orientation ($\{100\}$-$\langle 011\rangle$ crack system [15]) were determined to be $12.5\,\mathrm{MPa\,m^{1/2}}$ (second unloading step) and $12.8\,\mathrm{MPa\,m^{1/2}}$ (linear fit of initial and final part of J–Δa curve).

It can be stated that the procedure using the intersection of two linear fits is too inaccurate at this stage. Actually, the results on J from this method should generally be lower compared to the results derived from the second unloading step, which was not found. Performing more unloading steps will deliver more accurate fracture resistance curves for both J–Δa and CTOD–Δa. The variation of sample thickness, W, and crack length, a, should then permit to determine the fracture resistance value, which causes instable fracture in macro samples. Furthermore, the transition from fracture stage I to stage II, which indicates initiation of crack propagation, would become more clearly visible. This might be the point where instable fracture in macro samples occurs.

It was demonstrated with these experiments that unloading steps for the determination of crack extension are necessary for both J–Δa and CTOD–Δa curves. A large number of SE micrographs could also serve for the determination of crack length. However, at the initial stage of crack extension, tunneling of the crack in the center of the specimen seems to take place. Consequently, crack lengths from SE micrograph will underestimate the crack length, if crack growth is visible at all. As shown in Figure 4, crack lengths determined by unloading stiffness and SE measurements coincide in the later stage of the experiments. Thus, a certain number of unloading steps is advisable and with a higher number of steps, an increased accuracy in the determination of the start of crack growth can be expected. For a higher number of steps, there will probably be two unloading steps at the initial stage of the experiment indicating the same compliance of the cantilever. This in turn leads to a lower limit of J, where no crack propagation took place. Due to the lack of two unloading steps having the same slope, only an upper limit for toughness at crack initiation can be given here.

A fact that becomes very obvious when looking at Figure 5c is that all fracture mechanics approaches, no matter if linear elastic or elastic plastic results, reflect the increase of fracture toughness with increasing angle between notch plane and the crystal's cleavage plane, which is as expected. Fracture toughness values may vary with the chosen experimental setup (e.g. sample size, applied stress states) and the carried out evaluation. However, the above-mentioned increase in toughness demonstrates that the method of micro-cantilever testing is suitable to distinguish between brittle and tough materials in an absolute way.

Fracture experiments on naturally cracked cantilevers again show that LEFM gives lower limits for K_Q. Therefore, the J-integral evaluation was conducted. Absolute quantities cannot and should not be given due to the short bending length in relation to W. The crack length over specimen thickness is not constant and the crack experiences mixed mode loading conditions. Nevertheless, values for fracture toughness and J-values are in the same range as it was found for smaller FIB-notched cantilevers. Concluding, both FIB-notches of adequate notch root radius and natural cracks lead to comparable results.

6. Conclusion

Fracture experiments using notched micrometer-sized samples have been performed. One batch of samples was produced with the ion slicing technique and the FIB. A second batch of samples incorporating natural cracks was cut out of the bulk material using just the FIB. Fracture never occurred by a single, catastrophic event but instead stable crack growth was observed. Two different stages of crack growth were found for FIB-notched cantilevers. The first stage is comprised of crack tip blunting with a small amount of crack propagation. The local crack tip opening angle increases with increasing deviation of FIB-made notch from the dedicated cleavage plane. In the second stage, the crack continues to propagate in a stable manner. The local crack tip opening angle in the second stage is significantly smaller compared to stage I. The observed stable fracture can be explained by the lack of large volumes accommodating elastically stored energy and, consequently, the elastic energy release rate is lower.

Due to the large plastic zone in front of the crack tip leading to large scale yielding, linear elastic fracture mechanics, as it was applied for many other experiments of this kind using different materials, does not lead to correct results. However, LEFM gives a lower limit for critical fracture toughness values. *J*-values give the largest values for fracture toughness. CTOD was determined basing on a hinge model and the resulting fracture toughness values agree best with the results from macroscopically large samples that were taken from literature.

Disclaimer

This work, supported by the European Commission under the Contract of Association between EURATOM and the Austrian Academy of Sciences, was carried out within the framework of the European Fusion Development Agreement. The views and opinions expressed herein do not necessarily reflect those of the European Commission.

Acknowledgements

The authors thank Prof. Monika Jenko at the Institute of Metals and Technology (Ljubljana, Slovenia) for performing the ion slicing sample preparation. S.W. appreciates fruitful discussions with A. Hohenwarter.

References

[1] T.P. Halford, K. Takashima, Y. Higo and P. Bowen, Fatig. Fract. Eng. Mater. Struct. 28 (2005) p.695.
[2] D. Miyaguchi, M. Otsu, K. Takashima and M. Takeyama, Mater. Res. Soc. Symp. Proc. 1128 (2009) p.197.
[3] D. Di Maio and S.G. Roberts, J. Mater. Res. 20 (2005) p.299.
[4] S. Massl, W. Thomma, J. Keckes and R. Pippan, Acta Mater. 57 (2009) p.1768.
[5] K. Takashima and Y. Higo, Fatig. Fract. Eng. Mater. Struct. 28 (2005) p.703.

[6] K. Matoy, H. Schönherr, T. Detzel, T. Schöberl, R. Pippan, C. Motz and G. Dehm, Thin Solid Films 518 (2009) p.247.
[7] *ASTM Standard E399-09*, ASTM International, West Conshohocken, PA, 2003.
[8] A.A. Griffith, Phil. Trans.: Math. Phys. Eng. Sci. 221 (1920) p.163.
[9] D.E.J. Armstrong, M.E. Rogers and S.G. Roberts, Scripta Mater. 61 (2009) p.741.
[10] D.E.J. Armstrong, A.J. Wilkinson and S.G. Roberts, Phil. Mag. Lett. 91 (2011) p.394.
[11] K. Matoy, H. Schönherr, T. Detzel and D. Dehm, Thin Solid Films 518 (2010) p.5796.
[12] R.H. Schnitzel, J. Less-Common Met. 8 (1965) p.81.
[13] S. Wurster, C. Motz, M. Jenko and R. Pippan, Adv. Eng. Mater. 12 (2010) p.61.
[14] J. Riedle, P. Gumbsch and H.F. Fischmeister, Phys. Rev. Lett. 76 (1996) p.3594.
[15] J. Riedle, Bruchwiderstand in Wolfram-Einkristallen: Einfluβ der kristallographischen Orientierung, der Temperatur und der Lastrate (in German). PhD thesis, University of Stuttgart, 1995.
[16] M.D. Uchic, D.M. Dimiduk, J.N. Florando and W.D. Nix, Science 305 (2004) p.986.
[17] N.A. Fleck, G.M. Muller, M.F. Ashby and J.W. Hutchinson, Acta Metall. Mater. 42 (1994) p.475.
[18] C. Motz, T. Schöberl and R. Pippan, Acta Mater. 53 (2005) p.4269.
[19] J.R. Greer and W.D. Nix, Phys. Rev. B 73 (2006) p.245410.
[20] W.D. Nix, J.R. Greer, G. Feng and E.T. Lilleodden, Thin Solid Films 515 (2007) p.3152.
[21] S. Shim, H. Bei, M.K. Miller, G.M. Phar and E.P. George, Acta Mater. 57 (2009) p.503.
[22] D. Kiener, C. Motz, M. Rester, M. Jenko and G. Dehm, Mater. Sci. Eng. A 459 (2007) p.262.
[23] *ESIS Recommendations for Determining the Fracture Resistance of Ductile Materials*, ESIS P1-92, European Structural Integrity Society, 1992. Available at http://www.structuralintegrity.eu/documents/downloads/categories/3.html
[24] *ASTM Standard E 1820-99a*, ASTM International, West Conshohocken, PA, 2003.
[25] *Methods for Crack Opening Displacement (COD) Testing*, DD 19:1972, British Standards Institution, London, 1972.
[26] *ASTM Standard E 813-89*, ASTM International, West Conshohocken, PA, 2003.
[27] D. Hull, P. Beardmore and A. Valintine, Phil. Mag. 12 (1965) p.1021.
[28] J.M. Liu and B.W. Shen, Scripta Metall. 17 (1983) p.635.
[29] S. Wurster, C. Motz and R. Pippan, in *Proceedings of the 18th European Conference on Fracture*, Dresden, 2010.
[30] C.F. Shih, J. Mech. Phys. Solid 29 (1981) p.305.
[31] P.B. Hirsch, A.S. Booth, M. Ellis and S.G. Roberts, Scripta Metall. Mater. 27 (1992) p.1723.
[32] S. Kohlhoff, P. Gumbsch and H.F. Fischmeister, Phil. Mag. A 64 (1991) p.851.

Appendix

Corrections of force–displacement signals

The measured load vs. displacement curves (Figure 2a) were corrected with respect to the compliance of the lamella where the cantilevers are located on, which was already done in [29]. A second correction has to be made regarding the indentation depth. In the ideal case, the cantilevers' support base should not show a translation due to the application of force, however, it is not always the case. During the *in-situ* experiments, many images are made and by fitting the displacement of the support at a certain force by a straight line, it is possible to determine a quantity equivalent to the spring constant of the lamella. This was done for (S1) and (S2) resulting in 12.8 mN/μm for (S1), and 9.7 mN/μm for S2 [29]. Detailed *in-situ* observation of specimens (S3) and (S4) focused on the notched area, where the crack evolved. No spring constants could have been determined for these experiments. However, as the

specimens are positioned next to each other on the same ion-sliced lamella, a reasonable corrective value of 11 mN/μm was chosen for (S3) and (S4).

Furthermore, the recorded indenter displacement has to be corrected to take into account the generation of an indent. Four indentation depths vs. load curves were recorded with the same indenter in bulk single crystalline tungsten and a quadratic fit of the initial part of the loading curve was used to correct for the generation of an indent. This leads, as for the lamella-related correction mentioned above, to a decrease in the resulting cantilever displacement. Ideally, the combination of both corrections results in the force vs. displacement curves of a cantilever experiencing no indentation and sitting on an infinitely stiff support.

Determination of crack lengths

Several unloading steps were made to determine crack growth for each sample; this can be seen in Figure 2. The stiffness of the cantilever decreases when the crack grows. Hence, the ligament length $(W - a_i)$ in the ith step of unloading can be calculated according to the deflection of a cantilever:

$$W - a_i = \sqrt[3]{\frac{4kL^3}{BE}}, \tag{A1}$$

with k being the unloading compliance from the corrected load vs. displacement diagrams and E being the Young's Modulus, which was set to 400 GPa. Equation (A1) is valid for a one-side fixed cantilever with a thickness of $(W - a_i)$ and bending length L. The small distance from the notch to the cantilever's base, as well as the overall thickness W, was not taken into account. Using Equation (A1) the other way round, with the notch length determined in the SEM for (S1), (S2) and (S4), which can be found in Table 2, the nearly isotropic Young's modulus for tungsten single crystal is determined to be between 470 GPa and 550 GPa.

Equation (A1) is a rather rough assumption. Nevertheless, the results from calculations and direct observations agree, as can be seen in Figure 4. This figure shows that for small crack extensions, the crack lengths determined on the specimens' surfaces tend to be lower than the unloading stiffness would indicate. This might be because of tunneling of the crack in the center of the specimen for short crack extensions. In a later stage, after the crack extension approached the surface, crack lengths from SE micrographs approach the ones derived from unloading stiffness. The largest difference in crack lengths appears for cantilever (S4) which might be related to a larger amount of crack tunneling in the sample's center. Comparing the starting crack lengths: The calculated crack lengths from the first unloading step, a_1, where hardly any or no crack propagation took place, do not differ by more than 300 nm from the length of the FIB-notches for (S1), (S2) and (S4). Initial crack lengths were measured post-mortem in the SEM as FIB-made notches are easily distinguishable from fracture surfaces.